1

Introduction

Peng Cai, Wentao Deng, Hongshuai Hou, Guoqiang Zou, and Xiaobo Ji

Central South University, College of Chemistry and Chemical Engineering, No. 932, Lushan South Road, Yuelu District, Changsha 410083, China

1.1 A Brief Development of SICs

Nowadays, with the rapid development of daily household appliances, portable instruments, data storage systems, and aerospace facilities, it is even more necessary to develop new energy storage devices with high energy density, high power density, and good cycle stability. In the past, many researchers have been committed to designing excellent energy storage devices that take into account high energy density and high power density, such as rechargeable batteries and electrochemical supercapacitors (SCs) [1–13]. However, for the world, the configuration of electrochemical energy storage devices that provide both high energy density and high power has become an urgent need [14].

The successful commercialization of lithium-ion batteries (LIBs) in 1991 has received extensive attention from researchers [15–18]. LIBs are characterized by high working voltage, high energy density, and wide working voltage window but poor rate performance [19–22]. In comparison, SCs have higher power density and cycle stability, but their application is limited due to their low energy density defects [23, 24]. Therefore, in response to this defect, the concept of hybrid-ion capacitors was brought up [25–32]. In 2001, Amatucci used activated carbon (AC) to construct the first lithium hybrid capacitor as the cathode and nanostructured $Li_4Ti_5O_{12}$ (LTO) as the anode [17, 33, 34]. The energy density of the container is twice that of traditional carbon-based SCs, and at the same time it presents a bright magnification prospect. Since then, after the application of lithium hybrid capacitors in assembling a variety of devices, many researchers are still exploring and paying attention to the cost and future reserves of lithium, especially related to the application of large-scale energy devices and smart grids, and they have gradually proposed the idea of replacing lithium with sodium [32, 35–47]. In addition, there is another kind of alkali metal ion capacitor–potassium ion capacitor (PIC), which is rich in resources, but its related technology research is still in the preliminary exploration stage. There are five main factors restricting the development of

Sodium-Ion Capacitors: Mechanisms, Materials, and Technologies, First Edition.
Edited by Guoqiang Zou, Xiaobo Ji, and Hongshuai Hou.

PICs: (i) low ion diffusion rate in solid electrodes and poor potassium ion reaction kinetics; (ii) large volume changes during potassium insertion/depotassization; (iii) serious side reactions and electrolyte consumption; (iv) dendrite growth and safety hazards; and (v) limited energy density/power density caused by the relatively high atomic mass of *K*. In addition, some aqueous metal-ion capacitors (zinc-ion capacitors) have also received widespread attention. However, due to their lower energy density and longer cycle life, aqueous metal-ion capacitors are more suitable for applications in biological systems.

From the development of lithium-ion capacitors (LICs) and other hybrid-ion capacitors above, it is not difficult to see that mastering the development of LICs is very meaningful for researchers to explore the development of sodium-ion capacitors (SICs). Therefore, in order to better understand the development features and advantages of SICs, other types of hybrid-ion capacitors will be introduced in Section 1.2. Other hybrid-ion capacitors will be introduced in the categories of monovalent hybrid-ion capacitors and multivalent hybrid-ion capacitors. Taking the monovalent hybrid-ion capacitor as an example, the PICs are firstly introduced. Then, a brief introduction to multivalent hybrid-ion capacitors is given. For example: magnesium-ion hybrid capacitors (MICs), calcium-ion batteries (CIBs), zinc-ion hybrid capacitors (ZICs), and aluminum-ion hybrid capacitors (AICs). Compared with high power density, the core problems of these emerging systems may lie in other aspects. Therefore, these systems may not be fully developed in the field of hybrid-ion capacitors. Some basic thinking, attempts, and explorations of hybrid-ion capacitors in these emerging development fields will also be briefly covered. This chapter hopes to inspire readers to fully understand and master SICs by covering a variety of backgrounds and introductions. Table 1.1 and Figure 1.1 demonstrate the different characteristic aspects of the charge carriers of Li^+, Na^+, K^+, Mg^{2+}, Ca^{2+}, Zn^{2+}, and Al^{3+} for their respective energy storage systems.

As representative of monovalent hybrid-ion capacitors, LICs, their development history and successful commercialization path are worth discussing. In 1984, Dr. Yamabe of Kyoto University cooperated with Dr. Yata of Kanebo Co., Ltd. to synthesize a new type of carbonaceous material, namely polyacene semiconductor (PAS), by pyrolysis of phenolic resin [49]. In 1987, Yata et al. reported the intercalation/deintercalation properties of lithium ions in PAS, and research activities on LICs have received much attention since then [50]. In 2005, Fuji Heavy Industries was the first to commercialize LIC based on a porous carbon cathode and a pre-lithiated PAS anode with a stacked structure [51]. Since then, different companies have attempted to commercialize LICs based on various technologies, and a few promising commercial products are described in Table 1.2. Recently commercialized LICs can achieve gravimetric energy and power densities of 20 Wh kg^{-1} and 7.5 kW kg^{-1}, respectively, with lifetimes ranging from 100 000 to 800 000 [52].

Among the many LICs, the most classic is the pioneering work of Amatucci et al. As mentioned before, Amatucci et al. were the first to report LICs via hybridization of EDLCs and LIBs [33]. In 2001, AC(+)//$Li_4Ti_5O_{12}$(−) LIC using 1 M $LiPF_6$ in ethylene carbonate (EC)/dimethyl carbonate (DMC) (2 : 1, v/v) was first reported

Table 1.1 Characteristic physical properties of Li^+, Na^+, K^+, Mg^{2+}, Ca^{2+}, Zn^{2+}, and Al^{3+} ion carriers for hybrid-ion capacitors.

Properties	Li^+	Na^+	K^+	Mg^{2+}	Ca^{2+}	Zn^{2+}	Al^{3+}
Relative atomic mass	6.94	6.94	9.10	24.31	40.08	65.38	26.58
Mass-to-charge ratio	6.94	6.94	9.10	12.15	20.04	32.69	8.86
Theoretical gravimetric capacity of $ACoO_2$ ($mAh\,g^{-1}$)	274	235	206	260	242	–	268
Theoretical volumetric capacity of $ACoO_2$ ($mAh\,cm^{-3}$)	1378	1193	906	—	—	—	—
E^0 ($A/A^{n+}{}_{aq}$) V vs. SHE	−3.04	−2.71	−2.93	−2.37	−2.87	−0.76	−1.66
E^0 ($A/A^{n+}{}_{PC}$) V vs. $Li/Li^+{}_{PC}$	0	0.23	−0.09	—	—	—	—
Shannon's ionic radii (Å)	0.76	1.02	1.38	0.72	1	0.74	0.535
Stokes radii in H_2O (Å)	2.38	1.84	1.25	3.47	3.10	3.49	4.39
Stokes radii in PC (Å)	4.8	4.6	3.6	—	—	—	—
Molar ionic conductivity in PC ($S\,cm^2\,mol^{-1}$)	8.3	9.1	15.2	—	—	—	—
Molar ionic conductivity in $AClO_4$/PC ($S\,cm^2\,mol^{-1}$)	6.54	6.54	—	—	—	—	—
Polarization strength ($10^4\,pm^{-2}$)	2.16	1.11	—	4.73	—	—	—
Desolvation energy in PC ($kJ\,mol^{-1}$)	215.8	158.2	119.2	569.4	—	—	—
Melting point (°C)	180.5	97.8	63.4	650	842	419	660
Coordination preference (O = octahedral, T = tetrahedral, P = prismatic)	O and T	O and P	—	O and T	—	—	—

Source: Naskar et al. [48]/with permission of John Wiley & Sons.

by Amatucci et al. The LICs displayed sloping charge/discharge curves in the 1.5–3.0 V window with 90% capacity utilization at 10 C rate and 10–15% capacity loss after 5000 cycles. In their reports, the $Li_4Ti_5O_{12}$ anodes exhibit almost zero volume change upon Li^+ ion intercalation/deintercalation and show a terminal lithiation voltage of 1.55 V. In a follow-up publication in 2004, typical devices with 40 $Wh\,kg^{-1}$ large energy density and 4000 $W\,kg^{-1}$ high power density were developed by using nanostructured $Li_4Ti_5O_{12}$ anode and AC/$LiCoO_2$ composite cathode in 2 M $LiBF_4$/acetonitrile (AN) electrolyte [53]. High durability is achieved in this device due to the utilization of AC EDL cathode material and $Li_4Ti_5O_{12}$ nanostructured anode material. The capacity loss after 9000 cycles at full depth of discharge is 20%, which is quite superior compared to conventional LIBs.

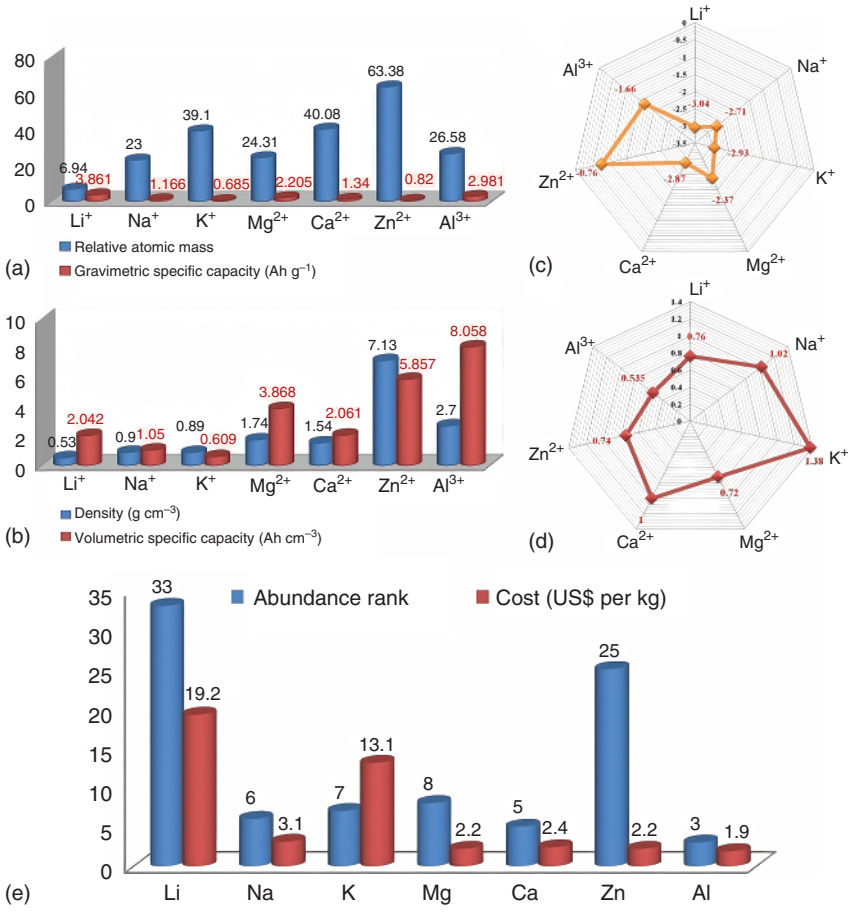

Figure 1.1 (a) Relative atomic mass and gravimetric specific capacity of metal. (b) Density and volumetric specific capacity of metal. (c) Standard electrode potential (V vs. SHE). (d) Shannon's ionic radii (Å) of different charge carriers for rechargeable batteries, and (e) Relative abundance-rank and cost of different charge carriers (Li^+, Na^+, K^+, Mg^{2+}, Ca^{2+}, Zn^{2+}, and Al^{3+}) for rechargeable batteries. Source: Reproduced with permission of Naskar et al. [48] Copyright 2021, Wiley-VCH GmbH.

1.2 Comparison Between Different Hybrid-Ion Capacitors

Similarly, among monovalent hybrid-ion capacitors, PICs have recently drawn attention as promising next-generation energy storage systems due to their relatively abundant potassium reserves and low cost. The development of PICs is accompanied by the development of potassium-ion batteries (PIBs). Since 2015, an increasing number of scientific publications on PIBs and PICs, can be observed. PICs exhibit some advantages [54]. For example, potassium does not thermodynamically form Al–K intermetallics, cheaper aluminum foils can be utilized as anode current

Table 1.2 Product characteristics of some of the most advanced commercial lithium-ion capacitors (LICs).

Company	Device type	Potential (V)	Capacitance (F)	Energy density (Wh kg^{-1})	Cycles
JM Energy Corporation	Prismatic	2.2–3.8	3300	13	300 000
General Capacitor Intl, Inc.	Laminate	2.2–3.8	3000	18	100 000
Taiyo Yuden	Cylinder	2.2–3.8	200	15	100 000
Vina Technology	Cylinder	2.2–3.8	270	—	—
Aowei Technology	Module	2.2–3.8	9000	>20	>30 000
Greenway	21 700	2.0–4.0	333	10.7	50 000
LRNET	Laminate	4	15 000	—	50 000
Asahi Kasei FDK energy	Module	15	600	12 Wh	—
ACT	Laminate	2.0–4.0	5000	15	—
NEC Tokin	Laminate	2.2–3.8	1000	8.0	—
MSR Micro	Laminate/ Prismatic	2.2–3.8	92–825 range	—	—
PuriXel, South Korea	Laminate	2.25–3.00	—	—	100 000

Source: Adapted from Naoi et al. [52].

collectors for PICs. Moreover, the standard electrode potential of K (−2.936 V vs. K^+/K) is lower than that of Na (−2.714 V vs. Na^+/Na), which may result in a wider voltage window, indicating higher energy density than SICs. Furthermore, due to the weak Lewis acidity of K^+, K^+ can form smaller solvated ions (3.6 Å) than Li^+ (4.8 Å) and Na^+ (4.6 Å) in monovalent hybrid-ion capacitors. Thus, PICs achieve fast ionic diffusion rates and high electrical conductivity in propylene carbonate (PC) solvent. Furthermore, unlike SICs, commercially available graphite can be used as anode materials for PICs by forming intercalation compounds (KC_8) with theoretical capacities of 279 mAh g^{-1}. Another significant advantage compared to SICs is that, for most anode materials, the intercalation potential of K ions is about 0.2 V relative to K^+/K, which reduces the possibility of metal potassium plating and effectively avoids the risk of dendrite formation during charging. For example, for hard carbon (HC) in SICs, the sodium potential is about 0.05 V relative to Na^+/Na, while for K^+/K in PICs, the potassium potential is 0.2 V. However, PICs also suffer from more limited cycling stability. Due to the large ionic radius of potassium ions (1.38 Å), among many electrode materials, especially the anodes would show large volume expansion during charge and discharge, resulting in a short lifespan in most PICs (usually <500 cycles). Consequently, more limited cycling stabilities are also great challenges for improving the power densities of PICs. Therefore, PICs are still in the developmental stages.

As discussed before, multivalent hybrid-ion capacitors may have a different focus than the core issues of monovalent hybrid-ion capacitors. To understand the features of MICs, a brief overview of the electrodes and electrolytes of MICs is required. As a divalent cation, energy systems based on Mg ions encounter sluggish kinetics due to the strong electrostatic interactions of Mg ions with anions in the host framework in the cathode. Therefore, the design of the cathode active material is a key factor. Chevrel phases ($Mg_xMo_6T_8$, T = S, Se, Te) and disulfides (MoS_2, WSe_2, etc.) are preferred as promising Mg-ion cathode active materials [55–59]; since in these host materials, the electrostatic interaction between Mg ions and anions is low. In addition, sufficient channel size in the crystal structure also facilitates the facile intercalation/deintercalation of Mg ions. On the other hand, moderately polar anions (S^{2-}, Se^{2-}, Te^{2-}, etc.) in electrode materials can lead to weaker bond strengths between transition metal cations, resulting in relatively low redox potentials for transition metals [60]. Therefore, Chevrel phases and disulfide show redox potentials below 2 V (vs. Mg^{2+}/Mg). This discussion suggests that higher voltages (i.e. higher energies) and fast kinetics (i.e. higher power) are not easily achieved simultaneously in MICs. Besides these materials V_2O_5 [61], MnO_2 [62], MoO_3 [63], $MgCo_2O_4$ [64], TiS_2 [65], TiO_2 [66], sulfur [67], iodine [68], and polyanion-based materials ($MgMnSiO_4$, $MgFeSiO_4$, etc.) [69, 70] have also been reported as cathode active materials for MICs. To better understand the properties of MICs, some characteristics of metallic magnesium anodes in magnesium-ion batteries (MIBs) are also introduced. From the anode point of view, metallic Mg electrode is a good choice for nonaqueous MIBs because of its high negative voltage (−2.37 V vs. SHE) and high theoretical capacity (2205 mAh kg^{-1}). However, complex reactions are prone to occur between the metal magnesium anodes and the electrolytes. Hence, the discussion of anodes and electrolytes needs to be covered. Due to the chemical activity of Mg in conventional electrolytes, it encounters serious problems: Due to the presence of Mg-ion salts in polar aprotic solvents, the Mg surface tends to form a hard passivation layer that inhibits ion pathways and accompanying electrochemical reactions. To circumvent this problem, researchers are turning to alloyed/dealloyed or Mg insertion/deintercalation types of anodes. However, such materials also suffer from slow kinetics and pulverization due to excessive volume changes during charge/discharge. Among alloying/dealloying materials, Bi, Sb, Bi–Sb, Ge, Si, Sn, and Sn-based binary alloys (Cu–Sn, Pb–Sn, and In–Sn) have been reported in the literature [71–74]. In addition, the development of non-Mg metal anodes has promoted the further development of MICs to a certain extent [75, 76]. In 2D materials, the anode of MICs can also use defective graphene and graphene allotrope moieties [77], black phosphorus [78], and $Li_4Ti_5O_{12}$ [79]. In organic systems, the development of MICs is mainly limited by electrolytes. Furthermore, a discussion of electrolytes in MIBs is essential when it comes to electrolytes for MICs. In the work of Aurbach et al., an unconventional electrolyte system based on organohaloaluminate magnesium salts in tetrahydrofuran (THF) and polyethers of the glyme was developed, in which metallic magnesium electrodes work reversibly with relatively fast kinetics [80]. Grignard reagents (RMgX; R: alkyl or aryl, X: Cl or Br) as electrolytes for MIBs have also

been reported in the literature for passivation-free metal Mg electrodes, but their strong reducibility limits the oxidative stability of cathodes [81]. Another electrolyte system, namely organoborate (magnesium dibutyldiphenyl $Mg(BPh_2Bu_2)_2$ and tributylphenyl $Mg(BPhBu_3)_2$) in THF (>0.4 mol), can realize anode reversible Mg stripping/plating as well as cathode reversible Mg ion insertion/extraction [82]. In recent years, MIBs of aqueous electrolytes have attracted attention due to their safe and cost-effective properties. For example, in 2019, Zhang et al. constructed devices based on δ-MnO_2@carbon molecular sieve composite as cathode and nanowire VO_2 as anode [83]. In 2017, Zhang et al. reported an aqueous anode with carbon-coated $FeVO_4$ and a todorokite-type magnesium octahedral molecular sieve (Mg-OMS-1) cathode [84]. Nam et al. proposed smart material engineering by introducing crystal H_2O into the layered structure of the brucite MnO_2 cathode to efficiently screen electrostatic interactions between Mg^{2+} and host framework anions [85]. The group also demonstrated lower desolvation energies at the cathode and electrolyte interfaces by adding H_2O to the nonaqueous electrolyte solution. This is because hydrated Mg ions are allowed to intercalate in their hydrated form, thereby minimizing desolvation energy loss. The intercalated hydrated Mg ions in the host framework further minimize the electrostatic interactions between Mg ions and host anions [86]. Therefore, the birnessite MnO_2 cathode in pure aqueous electrolyte exhibits a large reversible capacity of 231.1 mAh g^{-1} at 2.8 V.

However, the above overview of aqueous/nonaqueous electrode materials is used to complement the basic background of MICs. In 2014, Yoo et al. developed the first MICs utilizing AC cloth and magnesium metal as cathodes and anodes, respectively. To prevent hard passivation films and dendrite growth on the metal anodes, 0.25 M organohalide magnesium aluminate complexes ($Mg_2Cl_3^+$–$Ph_2AlCl_2^-$) were utilized in THF electrolytes [87]. In this electrolyte, the Mg electrode works reversibly for thousands of cycles with a CE of approximately 100%. On the other hand, the pores in the cathodes are saturated with large ions (bulky Mg and Al-based ionic complexes consisting of Cl, alkyl or aryl groups, and THF ligands) before the potential limit is reached. Surprisingly, the introduction of 0.5 M LiCl solves this problem, as small ionic substances will be present in the electrolytes. The full-cell device exhibited a specific capacitance of 90 F g^{-1} at 5 mA g^{-1} within 0.9–2.4 V and maintained 79% of the initial capacitance after 4500 charge/discharge cycles. In the following years, several researchers screened suitable materials and electrolyte systems for advanced MICs. Breakthroughs in MICs are more focused on aqueous electrolytes due to the significant challenges in organic systems. Sun et al. and Maitra et al. reported MnO_2 nanowires in $MgSO_4$/$Mg(NO_3)_2$ electrolytes and $MgNiO_2$/$Mg(ClO_4)_2$ electrolytes for low-cost aqueous MICs, respectively [88]. In 2017, Zhang et al. demonstrated aqueous MICs with (+)Mg-OMS-2/graphene//0.5 M $Mg(NO_3)_2$(aq)//AC(−) configuration [89]. The cryptomelane-type manganese oxide octahedral molecular sieves (OMS-2) are a unique electrode with 2×2 and 1×1 tunneling structures of MnO_2 in MICs, which is widely used as an active material in magnesium ion batteries. Besides, the low electronic conductivity of OMS-2 can be mitigated by the preparation of composites containing carbon material. The full cell exhibited a high energy density of 46.9 Wh kg^{-1} (100 mA g^{-1}) and excellent cycling stability

(95.8% capacity retention at 100 mA g^{-1} after 500 cycles) at 0–2 V. Cao et al. reported the utilization of Mn_3O_4 and AC as the active materials in cathode and anode, respectively, using aqueous electrolytes of 2 M $MgSO_4$ [90]. The MICs showed an energy density of 20.2 Wh kg^{-1} (125 W kg^{-1}) and excellent cycling stability (95% capacity retention after 6000 cycles at 0.5 A g^{-1}) with the potential of 0–2 V. In addition, the scaled-up flexible packaging depicts 80% capacity retention after 500 cycles at a current density of 0.5 A g^{-1}. Tian et al. reported Mg^{2+} ion insertion/detachment in neutral aqueous $MgSO_4$ electrolytes for VN anodes [91]. By increasing the scan rate from 1 to 200 mV s^{-1}, the rectangular-like CV and the small polarized redox peaks indicate the fast reaction kinetics due to a surface-controlled process. In order to understand the pseudocapacitance mechanism of VN during charging/discharging, both XPS and CV can confirm that the V(III) to V(II) transition is the key to the VN charge/discharge reaction. Quasi-solid aqueous MICs with a (+)MnO_2@C/$MgSO_4$ gel/VN(−) configuration show a bulk energy density of 13.10 mWh cm^{-3} (72 mW cm^{-3}), and a bulk power density of 440 mW cm^{-3} (10.35 mWh cm^{-3}) and excellent cycling stabilities (5000 cycles at 16 mA cm^{-2}) in the range of 0–2.2 V. In addition, the device was further developed as a flexible solar-charging integrated unit based on screen-printed micro-supercapacitors. However, the number of promising MIC systems is indeed limited from the point of view of laboratory prototypes or practical devices.

Possessing the highest Shannon's ionic radii of all multivalent charge carriers (Table 1.1), Ca^{2+} ions exhibit faster electrochemical reaction kinetics than Mg^{2+}, Zn^{2+}, and Al^{3+} ions, due to low polarization. However, as mentioned above, the promising classes of electrode materials for CICs are similar to MICs. Different experimental and simulation studies have shown that 3D tunneling and layered structures, such as $CaMn_2O_4$, V_2O_5, graphite, etc., are suitable for Ca^{2+} intercalation/de-intercalation. Therefore, these materials can be considered as anode materials for CICs. Inspired by the Mg^{2+} ion system, a similar Chevral phase ($CaMo_6T_8$ [T = S, Se, Te]) is theoretically envisaged for the Ca^{2+} energy storage systems [92]. The operating voltage of $CaMo_6S_8$ is predicted to be 1.4 V (vs. Ca/Ca^{2+}). However, the diffusion of Ca^{2+} is slower in $CaMo_6S_8$ than that of Mg^{2+}. The diffusion energies of Mg^{2+} and Ca^{2+} in $CaMo_6Se_8$ are both lower than those of $CaMo_6S_8$. The diffusion energies of Ca^{2+} in Mo_6S_8 and Mo_6Se_8 are 780 and 520 meV, respectively, which are relatively higher than the diffusion energies of Mg^{2+} (270 and 180 meV for Mo_6S_8 and Mo_6Se_8, respectively). Based on the quantitative diffusion barrier limits for cell operation, the nanostructured Mo_6Se_8 could be promising as a suitable anode for CICs with an average voltage of 1.25 V. However, no experimental data on the insertion/deinsertion of Ca^{2+} ions based on the Chevral phase are available in the literature to date. Cubic framework structures of Prussian blue analogues ($A_xMFe(CN)_6 \cdot yH_2O$ [where A = Li, Na, K, Mg, Ca, etc., and M = Ba, Ti, Mn, Fe, Co, or Ni]) have also been investigated as insertion electrodes for CICs, but their capacities are not up to the mark [93]. While Ca metal anodes may be attractive for CICs due to their high bulk and weight capacities, surface passivation and subsequent hard SEIs formation in conventional electrolytes hinders reversible Ca^{2+} stripping/plating. Therefore, in conventional

electrolytes (containing Ca ion salts in polar non-protonic solvents), an efficient Ca ion energy storage system cannot be achieved using metal anodes [94]. On the other hand, alloyed materials such as Ca–Sn and Ca–Si anodes can exhibit reversible alloying/dealloying electrochemical reactions with appreciable capacity by avoiding the formation of hard passivation films [93, 95]. In 1991, Aurbach et al. demonstrated the electrochemical behavior of Ca-metal electrodes in several organic electrolytes, such as $Ca(ClO_4)_2$, $Ca(BF_4)_2$, $LiAsF_6$, and tetrabutylammonium salts (BF_4^- and ClO_4^-) in THF, PC, AN, and γ-butyrolactone solvents [96]. During the electrochemical reduction of electrolyte solutions, $CaCl_2$ (in ClO_4^- salt solutions), $Ca(OH)_2$, $CaCO_3$, and calcium alcohol salts form passivation films which limit the reversible deposition/dissolution of electrodes in Ca-based nonaqueous electrolytes. In 2016, Ponrouch et al. reported that salts in organic electrolytes mixed with carbonate solvents (PC and EC) containing $Ca(ClO_4)_2$, $Ca(BF_4)_2$, and $Ca(TFSI)_2$ exhibited a wide electrochemical stability window at high temperatures (e.g. −0.5 to 3.5 V vs. Ca/Ca^{2+} at 100 °C) [94]. Ultimately, these electrolytes also show irreversibility of Ca^{2+} stripping/plating. In 2017, Wang et al. developed a THF-based electrolyte containing $Ca(BF_4)_2$ salt that can be operated at room temperature [97]. In this electrolyte, the reversible stripping/plating of Ca^{2+} was very satisfactory, but with lower anodic stability (3 V vs. Ca/Ca^{2+}) and lower CE. Unlike the reduction products that form hard SEIs in conventional electrolytes, CaH_2 was identified as the SEIs component in the THF-based electrolytes. Unfortunately, the SEI films were unstable and formed continuously during cycling due to CaH_2 deposition, resulting in a CE lower than that required for practical applications (99.98%). In 2019, Shyamsunder et al. synthesized a new fluorinated alkoxy borate ($Ca(B(Ohfip)_4)_2$·4DME), which is based on the hexafluoroisopropoxy ($Ohfip^-$) ligand [98]. It shows reversible stripping/plating of Ca^{2+} in 1,2-dimethoxyethane (DME) solvent at 25 °C with low polarization (170 mV). This salt also exhibits higher anodic stability up to 4.1 and 4.9 V in DME and *N,N*-dimethyltriflamide, respectively. In 2019, Li et al. reported a similar electrolyte system, calcium tetrakis(hexafluoroisopropoxy)borate ($Ca[B(hfip)_4]_2$) in DME, showing reversible stripping/plating of Ca^{2+} at room temperature with high oxidative stability up to 4.5 V vs. Ca/Ca^{2+} and high ionic conductivity (>8 mS cm^{-1}) [99]. Nevertheless, these electrolytes have some limitations and therefore require extensive research on the non-aqueous and aqueous electrolytes. Ta et al. and Lee et al. report computational simulation studies of Ca electrodeposition and species formation processes in nonaqueous electrolytes and modulate the hydration number of Ca^{2+} ions by varying the electrolyte concentration, respectively [100, 101]. Different theoretical and experimental studies on electrodes/electrolytes are essential in order to gain a more comprehensive knowledge on the feasibility of practical CICs. In 2019, Wu et al. reported the first CIC devices based on AC cathodes, Sn foil anodes, and a 0.8 M $Ca(PF_6)_2$ electrolyte solution in a mixed carbonate solvent (EC, PC, DMC, and EMC) [102]. During the charging of CICs, PF_6^- anions were adsorbed to the AC surface and Ca^{2+} were migrated toward the Sn anodes, forming the Ca_7Sn_6 alloy. During the discharge of CICs, the opposite process occurred. Based on the above mechanism, the full device exhibited an operating voltage of

1.5–4.8 V. Moreover, the CV curves at different scan rates (10–100 mV s^{-1}) indicated that the full-cell device delivers good CICs performances. Reversible capacities of 92 mAh g^{-1} (0.1 A g^{-1}) and 82 mAh g^{-1} (0.4 A g^{-1}) and a capacity retention rate of 84% over 1000 cycles at 0.2 A g^{-1} were achieved. To our knowledge, this is the only CIC device reported to date that shows promising electrochemical performances at room temperature.

ZICs are developed from ZIBs. ZIBs have received a lot of attention for their low cost, high safety, and environment friendliness. Typically, ZIBs consist of zinc metal anodes, aqueous electrolytes such as $ZnSO_4$ (aq), and cathodes for Zn^{2+} intercalation/de-intercalation. Unlike the extremely active lithium, sodium, and potassium metal electrodes, zinc metal electrodes are stable in air and can be used directly as the anodes in ZIBs. At the same time, metallic Zn electrodes have a high weight capacity of 823 mAh g^{-1} (corresponding to an ultra-high-volume capacity of 5845 Ah l^{-1}, much higher than 2046 Ah l^{-1} for lithium electrodes and 3833 Ah l^{-1} for Mg metal electrodes) and a low redox potential of −0.76 V compared to standard hydrogen electrodes [103]. In addition, the high ionic conductivity of the aqueous Zn^{2+}-containing electrolyte of the ZIBs facilitates fast charge/discharge rates. Therefore, ZICs inherit the excellent advantages of ZIBs. As mentioned above, the power density of the ZICs is highly competitive compared to other hybrid-ion capacitors. The two electrodes of ZICs (AC and Zn) are also very stable (in this neutral/light system) and ensure excellent cycling stabilities [104]. Most importantly, ZICs have the potential to be a hybrid ion capacitor device with good energy density, power density, and excellent long-term stabilities. ZICs typically utilize porous carbon (or AC) as the cathodes and zinc metal as the anodes. The highly reversible charge storage mechanism of the porous carbon cathode gives ZICs an extremely long service life. Zinc anodes store charge by plating and stripping, thus providing high capacity for ZICs. Given the low redox potential of the zinc anodes, aqueous ZICs with carbon-based cathodes can provide higher voltages (≈1.6–1.8 V) than symmetrical C//C SCs (≈1 V) [105]. Thanks to the hybrid configuration, ZICs can bridge the energy density gap between SCs and rechargeable batteries. In addition, ZICs offer more stable cycling performances and higher power densities than their ZIB counterparts. Based on the low cost of carbon materials and zinc metal, ZICs hold promise for low-cost and large-scale applications, especially for those requiring high power.

Research work on ZICs has only recently begun. In 2016, Wang and coworkers reported the first ZICs assembled from oxidized carbon nanotube cathodes and zinc anodes in aqueous $ZnSO_4$ electrolytes [106]. The ZICs showed a low specific capacitance of 53 F g^{-1}, which was attributed to the low specific surface area (SSA) of the oCNT cathode (211 m^2 g^{-1}). In 2017, Tang and coworkers used porous carbon with a high SSA (3384 m^2 g^{-1}) as ZIC cathodes [107]. Such ZICs provide a capacitance of 170 F g^{-1} at a current density of 0.1 A g^{-1}, corresponding to an energy density of 52.7 Wh kg^{-1} at 1725 W kg^{-1}. In order to increase the energy density of ZICs, research work has attempted to expand the voltage window by optimizing the electrolyte. Typically, aqueous $ZnSO_4$ electrolyte-based ZICs have a voltage window of 0.2–1.8 V. In 2018, Wang et al. developed an ultra-high

concentration water-in-salt (WIS) electrolyte [108]. The WIS electrolyte consisted of 20 M (mol kg^{-1}) lithium bis(trifluoromethanesulfonyl)imide (LiTFSI) and 1 M $Zn(TFSI)_2$. The WIS electrolyte provided a wide voltage window with voltages up to 2.1 V supported by a highly stable WIS electrolyte, and achieved a high average CE of 99.7%. In 2019, Lu ad coworkers assembled ZICs with high energy density by employing nitrogen-doped graded porous carbon as cathodes [109]. The nitrogen dopant was shown to obtain pseudocapacitance by lowering the energy barrier for the formation of C—O—Zn bonding. In 2019, Zapien and coworkers fabricated the first flexible ZICs using polyacrylamide hydrogel electrolytes [110]. In 2020, Bimbo and coworkers introduced Ti_3C_2 MXene as an anode material for ZICs [111]. Ti_3C_2-based ZICs exhibited a high capacity of 189 mAh g^{-1} with capacity retention of 96% after 1000 cycles. Zhi and coworkers ZICs were fabricated using phosphene as the cathodes [112]. Phosphene cathodes showed high capacitance of over 300 F g^{-1}. It was worth noting that pseudocapacitances can be used to increase the energy density of ZICs. Qu and coworkers improved the capacitance of ZICs by manipulating the ZICs in an oxygen reduction reaction [113]. Due to the oxygen reduction reaction, the discharge capacities of ZICs were much higher than their charging capacity. Alshareef et al. utilized hydrogen and oxygen pseudocapacitance to increase the capacitances of ZICs. These pseudocapacitance studies provide a new approach to the design of aqueous ZICs with high energy densities [114].

However, the development of practical ZICs requires overcoming multiple challenges [115]. One limitation is the low energy density, which can be improved by increasing the capacitances of the cathode materials and by widening the voltage windows. The voltage windows of ZICs are mainly driven by the electrochemical stabilities of the electrolytes. In alkaline electrolytes, the zinc metal interacts with hydroxide ions, resulting in the accumulation of zinc hydroxide materials on the zinc anodes. Isolated zinc hydroxide materials reduce the overall conductivity and increase the polarization of the zinc anodes. Therefore, alkaline electrolytes should be avoided in ZICs. In neutral and weakly acidic electrolytes (pH above 3), the voltage windows of ZICs are limited by parasitic reactions such as HER, OER, and oxidation of porous carbon cathodes. Another limitation of ZICs is the cycling stabilities of the zinc anodes. Compared to the carbon cathodes, zinc anodes exhibit limited cycling stabilities due to dendrite growth, HER, and corrosion reactions. The formation of zinc dendrites involves a complex process, which is highly dependent on the inhomogeneous electric fields and ion distributions. During charging and discharging, the growth of zinc dendrites increases the SSA of the zinc anodes, thereby accelerating the HER rates. The high HER rate consumes protons in the aqueous electrolytes, leading to the accumulation of hydroxide ions. The hydroxide ions interact with the zinc anode and thus trigger the zinc corrosion reactions. Zinc corrosion results in the accumulation of zinc hydroxide substances on the surfaces of the zinc anodes. These byproducts reduce the overall electrical conductivity and exacerbate the inhomogeneous electric field of the zinc anodes, thereby increasing dendrite growth. Subsequently, the vicious cycles of zinc dendrites, HER, and zinc corrosion continue. Besides metallic zinc anodes, the modification of porous carbon electrodes is also a concern. The capacitances of porous carbon cathodes have

been improved by porous structure engineering and pseudocapacitive engineering. Advanced capacitive cathode materials, such as MXenes, phosphorene, and TiN, have proved to be promising candidates for cathode materials for ZICs. In addition to electrodes, the design of electrolytes is also a core area. Aqueous $ZnSO_4$ solutions are the most widely used electrolytes in ZICs. ZIC electrolytes containing $ZnSO_4$ aqueous solutions have a limited voltage window of 0.2–1.8 V. Beyond this voltage range, the electrolyte is subjected to a number of different types of electrodes. Beyond this voltage range, parasitic reactions, such as HER, can occur and damage ZIC devices. To suppress parasitic reactions and expand the voltage window, the electrolyte composition, such as substance, concentration, and solvent, can be optimized. In addition, zinc anodes exhibit poor cycling stabilities compared to porous carbon cathodes, which have an extremely long cycle life. In the case of zinc anodes, the growth of zinc dendrites, ion distributors, and artificial SEIs is suppressed by expanding the electrochemical surface area with a 3D architectural design. The use of low-potential intercalation anodes also helps to avoid zinc dendrite growth.

Despite the research results achieved with ZICs, the current results are based on laboratory-scale devices and focus on specific components rather than complete devices. In the reported ZICs, the capacities of the anodes, cathodes, and electrolytes do not match. For studies of ZICs, zinc anodes and electrolytes are often used in excess. The reported energy densities of ZICs are unreliable, as these values are based on the active mass of the porous carbon cathodes. Further research should therefore focus on capacity matching between anodes and cathodes. In other words, the utilization of zinc should be as high as possible. Cycle life, energy density, and power density are only meaningful if there is a limited use of zinc cathodes. From a practical point of view, the resource cost is an important parameter to prove the feasibility of ZIC devices in practical applications. Estimating the actual energy density and the corresponding capital cost of the device is necessary for the further development of ZICs. As the energy density of ZICs can be further increased by various engineering strategies, ZICs are promising energy storage technologies in the future energy storage market. Cost is one of the key parameters determining whether ZICs can be used for practical applications. Although porous carbon and ZICs have a good industrial base, the cost of commercial AC (US$ 57–114 per kg) is much higher than that of ZICs (US$ 2.1 per kg). Based on the above estimated data, the cost of electrode material for ZIC would be US$ 365.6 per kWh (US$ 7.2 per kWh for zinc anodes and US$ 358.4 per kWh for porous carbon cathodes) [116]. The high cost of porous carbon is therefore a bottleneck for the practical application of ZICs. In order to reduce the cost of ZICs, a simple low-cost porous carbon manufacturing process is required. It is believed that more green synthesis processes will be developed for low-cost porous carbon materials. The last few years have seen tremendous progress in the electrochemical performances of ZICs. In future, a great deal of effort should be put into the manufacture of ZICs for practical applications. In the next few decades, there will be numerous potential opportunities to scale up ZICs with high performances.

As three-electron redox systems (Al/Al^{3+}), energy storage devices based on aluminum ions have a higher theoretical capacity and higher energy density. However,

due to the higher polarization, the trivalent Al^{3+} suffers from a higher desolvation energy and a higher solid-state diffusion energy barrier. Considering the ease of practical devices based on divalent ions (Mg^{2+}, Ca^{2+}, and Zn^{2+}), trivalent ions (Al^{3+}) are expected to be more difficult. However, the first reported use of aluminum metal as anodes dates back to 1857, and the concept of AIBs for aluminum ion batteries was introduced in 1972 [117]. Since then, researchers have been working to develop practical aluminum-based devices by finding solutions for screening suitable cathode active materials with easy Al^{3+} ion diffusion (solid state), finding suitable cathode active materials for aqueous and nonaqueous media, optimizing the electrolytes for lower desolventization energy, and minimizing the formation of hard SEIs on aluminum metal electrodes. Therefore, the correct choice of electrolyte composition is key to the success of AICs. Aqueous salt electrolytes with $AlCl_3$ or $Al_2(SO_4)_3$ cannot be used for Al anodes because of the formation of Al_2O_3 through surface passivation and the intrinsic hydrogen precipitation reaction. Nonaqueous electrolytes can overcome these limitations. Historically, binary ($NaCl–AlCl_3$) and ternary ($KCl–NaCl–AlCl_3$) molten salts have been used as possible electrolytes; however, Al^{3+} is not present [118]. This chloroaluminate molten salt electrolyte system is divided into three parts, viz. acidic, neutral, and basic species, based on the molar concentration of $AlCl_3$. Molar concentrations of $AlCl_3$ of less than 50% in the electrolyte provide the basic characteristics by containing $AlCl_4^-$ and Cl^- primary anions, while more than 50% provides an acidic electrolyte with $AlCl_4^-$ and $Al_2Cl_7^-$ anions. There is evidence that reversible Al electrochemical stripping/plating occurs only in acidic compositions [119]. However, the high melting point of such molten chloride aluminate electrolytes limits their practical application. On the other hand, fluorinated salts in organic solvents are not suitable for aluminum-based systems, but this is negligible for lithium/sodium/potassium-based systems. For example, aluminum salts containing fluoride anions in the electrolyte (similar to $LiPF_6$ in LICs) form electronically and ionically nonconductive passivated AlF_3 layers on aluminum metal electrodes, which hinders the reversibility of aluminum stripping/plating. At the same time, high desolvation energy losses at the electrode/electrolyte interface increase the polarization of the electrochemical reactions in typical organic systems (e.g. ethers). These problems are responsible for the slow kinetics of AICs using conventional fluorinated electrolytes in organic media. Recent research and developments have shown that ILs with high ionic conductivity, low volatility, and high chemical/electrochemical stability can be used as electrolyte solvents in AICs at room temperature [120]. Common IL-based electrolytes are prepared by mixing $AlCl_3$ with imidazolium chloride in a specific ratio. The most commonly used imidazolium chlorides are 1-butyl-3-methylimidazolium chloride ([BMIM]Cl) and 1-ethyl-3-methylimidazolium chloride ([EMIM]Cl). Herein, the Lewis acidity of the electrolyte is achieved by maintaining the molar ratio of $AlCl_3$/imidazolium salt greater than one. The reaction mechanism for aluminum stripping/plating is similar to that of the molten chloroaluminate electrolyte described above in terms of the main anion species and reversible reactions. Therefore, in the cathodes in AICs devices, graphite-based materials (3D graphite foam, graphene microflower, etc.), metal sulfides (Mo_6S_8, FeS_2, SnS_2, Ni_3S_2, CuS,

Co_9S_8, etc.), metal oxides (TiO_2, V_2O_5, etc.), Prussian blue analogues (CuHCF), MXene (V_2CT_x), chloroaluminate-doped conductive polymers, etc. have been well reported [52]. Due to their high bulk density, high abundance, and environment friendliness, aluminum metal anodes are mostly accepted by conventional AICs. Notably, after removal of the surface oxide films, the thin Al_2O_3 films in commercial aluminum foils show better electrochemical properties compared to pure aluminum foils [52]. The defective sites in the oxide films facilitate efficient penetration of the electrolytes and minimize dendrite growth. In aqueous aluminum-based systems, surface modification of aluminum foils by ionic liquid impregnation introduces artificial SEIs to minimize hard surface passivation on the aluminum anodes. Salt-packed aqueous or solid/quasi-solid electrolytes are also suitable for aqueous AICs, while the overpotential of the hydrogen precipitation reaction is significantly increased [52]. Interestingly, in addition to aluminum metal electrodes, zinc metal, MoO_3@PPy nanotubes, SWCNT/$W_{18}O_{49}$ nanowires, etc. have also been tried as anode materials in aqueous AICs.

In 2016, Yoo et al. filed a US patent for AICs by preferentially using aluminum (including aluminum foil, aluminum powder, aluminum foam, shell particles with an aluminum coating, and aluminum alloys) anodes, and high surface area porous carbon (including AC, CNT, and graphene) cathodes/[EMIM]Cl with $AlCl_3$ electrolytes [121]. According to the patent description, in addition to aluminum metal, graphite, aluminum-doped graphite, carbon, silicon, titanium dioxide, molybdenum sulfide, and other intercalation/de-intercalation materials can also be used as potential anodes. Similarly, conductive polymers, oxides, sulfides, and nitrides are also suitable for potential cathodes. The patent description is not limited to electrolytes in ionic liquids; it also includes organic/aqueous electrolytes and even solid electrolytes. Tian and his colleagues developed low-cost and high-performance aqueous AICs by using nanostructured V_2O_5-impregnated mesoporous carbon microspheres (MCM/V_2O_5) in a 1 M $Al_2(SO_4)_3$ electrolyte. The AICs operated through the intercalation/de-intercalation of Al^{3+} and the reduction/oxidation of V^{5+}/V^{4+} pairs. The CV of the AICs showed typical redox properties due to the pseudocapacitance contribution of the V^{5+}/V^{4+} pair. The *b*-value of the composite electrodes (close to 1) indicated the dominant capacitance/pseudocapacitance contribution in the energy storage. The higher quality loading of V_2O_5 reduced the *b*-value, suggesting that V_2O_5 led to a diffusion-controlled mechanism. As-prepared AICs devices delivered an energy density of 13.2 Wh kg^{-1} (147 W kg^{-1}), a power density of 5840 W kg^{-1} (7 Wh kg^{-1}), and good cycling performances (capacitance retention of 90% after 10 000 cycles at 1 A g^{-1}) in the range of 0–1.6 V. The AICs designed by Lei et al. [122] were composed of nitrogen-doped graphene as the cathode materials, aluminum foil as the anode materials, glass fibers as the separators, and [EMIM]Cl/$AlCl_3$ as the electrolytes. In this device, the capacitive behaviors were derived from the adsorption/desorption of $AlCl_4^-$ ions in the nitrogen-doped graphene. The rectangular CV curves of the hybrid devices at various scan rates indicated that the nitrogen-doped graphene exhibited good properties in AICs. In addition, a weak reduction peak at 1.9 V indicated the presence of $AlCl_4^-$ intercalation/de-intercalation in/from the layer structures. The AICs device

showed an initial discharge capacitance of 160 F g^{-1} (95% CE at 0.3 A g^{-1} within 0.3–2.3 V) increasing to 254 F g^{-1} (90% CE) after 1000 cycles. The nitrogen-doped graphene cathode was activated in the first 30 cycles, after which the capacitance showed a slow increase up to 1000 cycles. Wang et al. reported AICs with a (+)AC//0.5 M $Al_2(SO_4)_3$(aq)//PPy@MoO_3(−) structures [123]. CV curves for the full devices of the AICs showed broad peaks associated with the intercalation/de-intercalation of Al^{3+} into/out of MoO_3@PPy. *b* values (0.5) also demonstrated the solid-state diffusion kinetics of MoO_3 in the $Al_2(SO_4)_3$ electrolytes. The device exhibited an energy density of 28 Wh kg^{-1} (460 W kg^{-1}), a power density of 2840 W kg^{-1} (20 Wh kg^{-1}), and good cycling performances (93% capacitance retention after 1800 cycles at 2 A g^{-1}) in the 0–1.5 V. Considerable electrochemical performances are achieved due to the PPy coating and the nanotube structure of MoO_3. PPy provides a conductive network with reduced charge transfer resistance and also protects MoO_3 from acid etching (acid can be produced by hydrolysis of $Al_2(SO_4)_3$). The nanotube structure facilitates the penetration of electrolytes and buffers MoO_3 volume changes due to Al^{3+} intercalation/de-intercalation. Furthermore, the fabricated (+)AC//PPy@MoO_3(−) devices were able to light up red LEDs, which demonstrated the practicality of the devices. Li et al. reported flexible AICs with (+)SWCNT/PANI//1 M $AlCl_3$ (aq)//SWCNT/$W_{18}O_{49}$(−) [124]. The CV curves of SWCNT/$W_{18}O_{49}$ composites revealed broad redox peaks due to the fast pseudocapacitive reactions. This unique network structure contributed to fast ion transport and provided high electrode conductivity (1626 S cm^{-1}). In addition, the $W_{18}O_{49}$ nanowires exhibited a wide lattice spacing, high aspect ratio, and homogeneous laminar structures, which facilitated the efficient intercalation of Al^{3+} ions. On the other hand, the SWCNT/PANI cathode provided a combination of capacitive/pseudocapacitive mechanisms. The hybrid device showed a bulk energy density of 19.0 mWh cm^{-3} (295 mW cm^{-3}), a bulk power density of 1278 mW cm^{-3} (14.5 mWh cm^{-3}), and an excellent cycling stability (95.9% capacitance retention at 14 mA cm^{-2} after 6000 cycles) at 0–1.8 V. Nevertheless, the number of successful AICs reported in the literature is indeed limited.

Now turn our attention back to the SICs. Both sodium and lithium are elements of the first main group, and their chemical properties are similar. Although the radius of sodium ions is larger than that of lithium ion (0.102 vs. 0.076 nm), the resource reserves of lithium ions are far behind those of sodium ions [125–132]. Sodium is one of the most abundant elements in the earth's crust, about 2.74%, ranking sixth. And when sodium ions are dissolved in H_2O, the radius is relatively small (compared with potassium ions), and it diffuses in H_2O faster than other ions, so the conductivity of sodium ions in the solution is higher [133]. Musashi Energy Solutions Co., Ltd. pointed out that SICs can be used in many fields such as construction machinery, photovoltaics, wind farms, and medical machinery. Although the solid-state diffusion in the electrode material lattice often determines the rate of traditional batteries, sodium ion energy storage devices may change this trend and generate better power than LIBs [134–136]. Therefore, in the long run, the development of sodium-ion capacitors is very promising. Therefore, SICs, as an emerging technology, are considered to be a supplement and extension to existing LICs [137, 138].

In 2012, Kuratani and coworkers developed an SIC energy storage device with hard carbon (HC) as the anode and AC as the cathode. Since then, the research of SICs has developed rapidly. Surprisingly, the energy density of SICs is 20–50 times greater than that of traditional capacitors, and the power density of SICs is 20–40 times greater than that of traditional sodium ion batteries (SIBs) [138–146]. Therefore, SICs can bridge the gap between SIBs and SCs [147, 148]. Compared with traditional SCs, the energy density of SICs is up to four times higher, so mechanical devices used for regenerative braking may be significantly beneficial. In the past few decades, different materials have also been used to enhance the energy storage performance of SIC, and these concepts are gradually deviating from the concept of classic SIC. Therefore, it is of great significance to classify SIC and clarify different energy storage mechanisms in the current context [149–153]. Therefore, it is very important to build high-performance SIC devices based on an in-depth understanding of the mechanism.

1.3 SICs Energy Storage Mechanism Introduction

In order to improve the performance of the cathode and anode, scholars will further explore and study pseudocapacitance materials in SIC devices [154]. On the one hand, many studies will focus on how to use pseudocapacitive materials to replace the traditional EDLC-type cathodes and further assemble them with battery materials to realize hybrid devices. SIC devices involving pseudocapacitor cathodes are in the middle position between EDLC cathodes and battery cathodes. Pseudocapacitance can be regarded as a supplementary mechanism of EDLC because it is not a mechanism of electrostatic adsorption, but compared to EDLC, pseudocapacitance has a similar CV curve shape and comparable constant CDC curves [155]. On the other hand, the pseudocapacitance material in the anode is also the main interest of SICs research. With the rapid development of anode nanotechnology and nanoscience, nanomaterial anodes have played an important role in electrochemical energy devices over the years. Nano-scale materials are small in size but large in surface area. In this case, it is impossible to accurately distinguish between surface and volume. Therefore, some anodes based on the Faraday mechanism usually exhibit strong redox reactions in the matrix. When the size is reduced to nanometers, they behave like pseudocapacitive materials, characterized by the disappearance of CV and CDC curves. Therefore, in recent years, the boundary between battery materials and pseudocapacitive materials has become blurred [156]. It should be noted that the misunderstanding of the confusing electrochemical energy storage mechanism will lead to the opaque development of controversial battery configurations (dual-ion battery configuration and dual-capacitor configuration) or SIC devices (flexible devices and prefabricated technology). Therefore, in addition to the chaotic mechanism, the neglected cell configuration and the newly developed flexible equipment and prefabricated areas were completely researched.

1.4 Key Technologies of SICs

SICs mainly consist of cathode/anode materials, collectors, electrolytes, separators, and metal shells. Among other things, the design of flexible devices and the development of pre-sodiation methods are the focus of future research into SIC devices. On the one hand, flexible electronics have revolutionized our lives and permeate every aspect of our daily life. Flexible energy storage devices are receiving increased attention due to their enormous potential in the emerging flexible electronics market, including roll-up displays, flexible mobile phones, skin sensors for human health monitoring, and implantable medical devices. The development of flexible SICs is important for the next generation of SIC devices. On the other hand, pre-sodiation methods are an integral part of electrochemical energy storage systems and can effectively compensate for irreversible capacity losses, increase the operating voltage, and improve the concentration of Na^+ in the electrolytes. Therefore, flexible SICs devices and pre-sodiation methods will be two important areas of key technologies for SICs devices. Both of these areas are important research areas for SICs devices and play a key role in driving the development of SICs devices.

The current energy storage devices are rigid and bulky and cannot meet the basic requirements of flexible energy storage. Therefore, efforts must be made to achieve structural optimization, light weight, and flexibility. A promising research direction is the development of lighter, smaller, and thinner modern flexible devices, including soft electronics, winding displays, and wearable products. This also requires advances in the corresponding energy supply devices. The development of flexible electrodes with low cost, high performance, good stability, safety, and reliability is a major challenge for many practical applications. The rapid development of portable electronic devices has contributed to the development of better electrochemical energy storage technologies. Flexible SIC devices are complex devices whose effective energy densities and cycling stabilities depend on various design factors, including the configuration and choice of electrolytes. Each of these factors plays a key role in improving electrochemical performance. In this chapter, several simple flexible SIC devices are classified according to the different configurations of SICs, which gives the reader a step ahead to familiarize themselves with the significance of the configuration and the simple development of flexible SIC devices. For this chapter, these introductions are important. A more detailed analysis and discussion can be studied in Chapter 7.

The first kind of flexible SIC device presented here consists of an EDLC-type cathode and a battery-type anode. For battery-type anodes, titanium-based composites, in particular $Na_2Ti_3O_7$ and $Na_2Ti_2O_{5-x}$, have been widely explored as attractive flexible materials due to their low potential and good electronic conductivity [157]. In the absence of binders or metal collectors, Zhang and coworkers developed flexible SIC devices based on $Na_2Ti_3O_7$ nanosheet arrays/CT anodes and flexible rGO film cathodes [158]. By a simple hydrothermal method combined with a subsequent calcination process, the $Na_2Ti_3O_7$ nanosheet arrays were grown directly on the CT and showed good adhesion. The synthesized material can be bent at arbitrary angles and has good flexibility. The whole device using nanostructured $Na_2Ti_3O_7$/CT

and rGO films as electrodes exhibits excellent electrochemical properties while maintaining good flexibility. The CDC curves of the flexible SICs devices can be recycled at different rates over a potential range of 1–3 V from 0.1 to 1.5 A g^{-1} and show stability at 0.5 A g^{-1} (over 80.3% of capacity after 2500 cycles) as well as higher coulombic efficiency (close to 100%). In another case, Gu and coworkers prepared flexible $Na_2Ti_2O_{5-x}$ electrodes and by introducing oxygen vacancies [159]. They assembled flexible SICs (labeled rGO/AC//$Na_2Ti_2O_{5-x}$@Ti//rGO/AC) using $Na_2Ti_2O_{5-x}$@Ti as the anodes and rGO/AC as the cathodes. The hybrid SIC devices offer high coulombic efficiency (close to 100%) and good cycling stabilities (82.5% capacity retention) at 1 A g^{-1} after 5000 cycles. The flexible SICs devices operate at potentials of 1–3.8 V and have maximum energy and power densities of 15.6 Wh l^{-1} and 120 W l^{-1}, respectively.

The flexible SIC devices presented in this place consist of cell-type cathodes and EDLC-type anodes. As for the EDLC-type anodes, research has mainly focused on AC. In order to provide high power characteristics, Fan et al. designed and fabricated a novel type of N-doped mesoporous carbon nanosheets (mp-CNS) consisting of interconnected Co/Zn metal organic framework (MOF) nanosheets [160]. In order to give the flexible SIC devices high power, the pseudocapacitive VO_2@mp-CNSs/CFC material is synthesized by depositing interconnected VO_2 on top of mp-CNSs/CFC. Flexible SIC devices are assembled from pseudocapacitive VO_2@mp-CNSs/CFC anodes and cellular NVP@mp-CNSs/CFC cathodes. At 1 A g^{-1}, the flexible SIC achieves a capacity retention of 78% after 2000 cycles. Furthermore, no significant structural damage was observed at different bending angles from 0° to 90°.

The above examples of flexible electrodes are innovative or improved in that there are no binders or collectors, but the electrolyte remains a conventional liquid organic electrolyte. In addition, most of the liquid organic electrolytes used in hybrid flexible SIC devices are highly volatile and flammable, posing a safety hazard. Therefore, effective solutions need to be proposed. Due to the low literature coverage in this area, only quasi-solid electrolytes are briefly discussed here. Fan et al. and Yu et al. used P(VDF-HFP) membranes to avoid these problems. Yu et al. used sea urchin-like $Na_2Ti_3O_7$, peanut shell-derived carbon (PSC), and P (VDF-HFP) membranes as anodes, cathodes, and electrolytes to construct flexible quasi-solid SICs [161]. Flexible $Na_2Ti_3O_7$//PSC quasi-solid SICs provided 86% capacitance retention and nearly 100% coulombic efficiency after 3000 cycles. The prepared $Na_2Ti_3O_7$//PSC quasi-solid state SICs devices showed no significant capacity loss under different bending conditions, confirming their superior mechanical strength. The flexible $Na_2Ti_3O_7$//PSC quasi-solid-state SIC devices can power up to 50 red LEDs and show both high power and high energy characteristics.

For flexible SIC devices, the concept of the configuration and the development of the electrolyte have been briefly outlined. The development of the relevant details will be provided in detail in Sections 7.1, 7.2, and 7.3. We believe that these discussions have given the reader a lot of insight. In addition to flexible SIC devices, another topic that cannot be avoided is the field of pre-sodiation methods in SICs. In pursuit of the growing demand for new applications with higher energy densities,

researchers have invested in and developed a large number of materials for energy storage electrodes. However, the associated pre-sodiation techniques have not received sufficient attention and have seriously hampered the commercialization of SIC devices. Pre-sodiation methods, i.e. the pre-doping of sodium ions, refer to the addition of a sodium source to the SIC devices to ensure sufficient sodium content. In general, pre-sodiation methods serve to compensate for the initial irreversible capacity loss of SIC devices. In a general sodium ion system, the storage and release of capacity is based on the reversible intercalation and de-intercalation of Na^+ in the electrode materials, while the Na^+ required for the anode is generated from the cathodes. During charging, a certain amount of active sodium is lost, mainly due to the formation of SEIs in the anodes. As a result, the irreversible sodium will decrease in the subsequent cycles. Surprisingly, the loss of active sodium content can be compensated by pre-sodiation methods to further ensure an increase in energy densities. In addition, pre-sodiation methods increase the operating voltage of SIC devices during cycling and reduce the consumption of electrolytes. Fortunately, various pre-sodiation methods have been successfully developed and work has been reported in recent years. Different pre-sodiation methods exhibit different mechanisms, which play a crucial role in the development of SICs. As fewer pre-sodiation methods have been reported for SICs devices, the main effective pre-sedimentation strategies are summarized as follows: (i) Direct contact methods; (ii) electrochemical methods; and (iii) adding additives methods. In different places, these names may be replaced by different expressions in different forms, but the underlying mechanisms are similar. Other similar or different examples are discussed in Chapter 8.

Direct contact methods: Moeez et al. developed a direct contact method to achieve presoaking of the electrodes and metal sodium, demonstrating an improved coulombic efficiency for the first cycle with improved cycle stability and reversible capacity [162]. In addition, a thick passivation layer is formed at the interface during the process; this helps to improve cycling stabilities by preventing dissolution of the active materials and deposition on the anode surfaces. The direct contact method is a simple and economical method of pre-sodiation, which has potential applications in practical production. To achieve contact, sodium metal is connected directly to the electrodes with a small amount of electrolytes (0.5 ml). Constant pressure is applied using, for example, plastic slides and adhesive clips so that the layered sodium metal is in good contact with the electrode and is maintained for 30 minutes. The sodium ions can enter the electrode at the same time and achieve charge neutrality. By bringing the sodium metal into contact with the electrodes, the sodium ions can be inserted into the active material to compensate for the initial loss of sodium. It is important to note that the measurement of the sodium metal and the open circuit voltage (OCV) is crucial to determine the degree of pre□sodium. In addition, the placement of a trace amount of electrolytes between the sodium metal and the electrode is important for the insertion of excess sodium ions in this pre-treatment. The electrolytes not only provide a bridge for sodium ions to migrate from the source to the

electrode, but also help to form a stable passivation layer between the electrodes and the electrolytes. The passivation layer protects the electrode materials from undesirable side reactions. In view of the high reactivity of sodium metal, all experiments should be carried out in Ar glove boxes at $H_2O < 0.1$ and $O_2 < 0.1$ levels.

Electrochemical methods: In the case of electrochemical methods, pre-sodiation methods are accomplished by cycling at relatively low current densities, where the sodium and targeted electrodes are isolated from each other. This method can be achieved by performing several charging and discharging cycles to achieve the desired potential. The process is short-circuit free, safe, green, and controllable, and opens up a new avenue of research in pretreatment technology. This method is currently the most widely used method. Zou et al. utilized the working electrodes, sodium metal electrodes, electrolytes, and separators to assemble a CR2016 cell under a high purity argon atmosphere [163]. The half-cell anode was cycled five times at $0.1\,A\,g^{-1}$. The sodium metal electrodes are then removed, and the SICs devices are assembled in a glove box with the cathode (working electrode) remaining. However, while the electrochemical method is technically controllable and easy to perform, the assembly/disassembly step of the cell pre-treatment adds cost and process complexity to commercialization.

Adding additives methods: A novel voltage-induced efficient in situ pre-sodiation method was successfully implemented by Zou et al. [164] through introducing an organic sodium salt ($Na_2C_6O_6$) as a sodium source as extra adding additives in the cathodes. In addition, $Na_2C_6O_6$ possesses a stable sodium–oxygen bond, and the decarbonization product cyclohexanedione in the electrolytes is neutral and soluble, which can ensure the forward decarbonization reaction. It is worth noting that sacrificing organic sodium salts has the advantages of abundant resources, low cost, and environment friendliness, which is conducive to promoting commercialization. In view of these advantages, the $Na_2C_6O_6$-added components exhibit excellent electrochemical properties. Furthermore, as an organic sodium salt, $Na_2C_6O_6$ is electrochemically unstable at high voltage and can provide an adequate source of sodium. To ensure the electrochemical behaviors of the $Na_2C_6O_6$ anode, the assembled half-cells were first evaluated. In the first cycle of the CV curve, there is a low intensity anodic peak at 3.60 V and a distinct anodic peak at 3.98 V with a maximum oxidation current. In addition, there is no peak in the cathodic section, which indicates that the extraction of sodium ions is mostly irreversible. In other words, the extracted sodium source enters the electrode and cannot be returned to the positive material. Also, in the second cycle that followed, the previous anodic peak disappeared completely, further verifying the irreversible reaction of the cathode. Furthermore, a specific capacity of $309.8\,mAh\,g^{-1}$ could be extracted from the $Na_2C_6O_6$ electrode at $25\,mA\,g^{-1}$, indicating that the additional specific capacity was caused by a side reaction. However, in the first subsequent GCD curve, only an exceptional discharge capacity of $24.9\,mAh\,g^{-1}$ can be obtained, which may be related to the side reactions or capacitive behaviors of the conducting carbon. The initial charging process is irreversible, which agrees well with the CV curves. The experimental

results show that the $Na_2C_6O_6$ electrodes exhibit high irreversible capacities and can provide abundant sources of sodium, which facilitates the utilization of the anodes. The organic sodium salt exhibits irreversible electrochemical properties at high potential, which can provide an abundant sodium source without any negative impact on the subsequent physical operation. The results also show that both the carbon and TiO_2 anodes have good electrochemical compatibility with $Na_2C_6O_6$. This rational strategy is expected to provide a potential method to greatly simplify the physical assembly process, which may significantly accelerate the commercialization of SICs.

The above results first systematically and comprehensively analyzed and compared the EDLC mechanism, the battery-type mechanism, and the confusion pseudocapacitance mechanism. Subsequently, the SIC battery configuration with different orientation mechanisms for the cathode and anode was discussed. In addition, the characteristics of electrode materials in different SIC battery configurations are further summarized. Finally, the key technologies and future developments in related fields are summarized. The above conclusion summarized the current research progress of SICs from multiple angles, established a basic understanding of SICs, and provided a solid theoretical basis for subsequent research.

References

1 Hou, H., Shao, L., Zhang, Y. et al. (2017). *Adv. Sci.* 4: 1600243.
2 Zou, G., Hou, H., Foster, C.W. et al. (2018). *Adv. Sci.* 5: 1800241.
3 Hou, H., Banks, C.E., Jing, M. et al. (2015). *Adv. Mater.* 27: 7861.
4 Ge, P., Hou, H., Cao, X. et al. (2018). *Adv. Sci.* 5: 1800080.
5 Wu, T., Zhang, C., Zou, G. et al. (2019). *Sci. China Mater.* 62: 1127.
6 Cao, D.P., Yin, C.L., Shi, D.R. et al. (2017). *Adv. Funct. Mater.* 27: 9.
7 Han, Y.L., Hu, J.L., Yin, C.L. et al. (2016). *J. Mater. Chem. A* 4: 7382.
8 Li, L., Wu, Z.P., Sun, H. et al. (2015). *ACS Nano* 9: 11342.
9 Lv, J.L., Liang, T.X., Yang, M. et al. (2017). *Composites, Part B* 123: 28.
10 Lv, J.L., Yang, M., Liang, T.X., and Miura, H. (2017). *Mater. Lett.* 197: 127.
11 Xu, M., Fei, L.F., Lu, W. et al. (2017). *Nano Energy* 35: 271.
12 Zhou, H.P. and Hu, J. (2017). *Mater. Lett.* 195: 26.
13 Cai, P., Zou, K.Y., Deng, X.L. et al. (2020). *Front. Chem.* 8: 11.
14 Brousse, T., Marchand, R., Taberna, P.L., and Simon, P. (2006). *J. Power Sources* 158: 571.
15 Konno, H., Kasashima, T., and Azumi, K. (2009). *J. Power Sources* 191: 623.
16 Li, J.M., Chang, K.H., and Hu, C.C. (1800). *Electrochem. Commun.* 2010: 12.
17 Aravindan, V., Gnanaraj, J., Lee, Y.S., and Madhavi, S. (2014). *Chem. Rev.* 114: 11619.
18 Cao, W.J., Li, Y.X., Fitch, B. et al. (2014). *J. Power Sources* 268: 841.
19 Jain, A., Aravindan, V., Jayaraman, S. et al. (2013). *Sci. Rep.* 3: 6.
20 Yang, Z.W., Guo, H.J., Li, X.H. et al. (2016). *J. Power Sources* 329: 339.
21 Sun, X.Z., Zhang, X., Zhang, H.T. et al. (2014). *J. Power Sources* 270: 318.

22 Gokhale, R., Aravindan, V., Yadav, P. et al. (2014). *Carbon* 80: 462.
23 Zhao, Y.J., Liu, J.Z., Horn, M. et al. (2018). *Sci. China Mater.* 61: 159.
24 Bispo-Fonseca, I., Aggar, J., Sarrazin, C. et al. (1999). *J. Power Sources* 79: 238.
25 Schroeder, M., Menne, S., Segalini, J. et al. (2014). *J. Power Sources* 266: 250.
26 Minakshi, M., Duraisamy, S., Tirupathi, P.R. et al. (2014). *Int. J. Electrochem. Sci.* 9: 5974.
27 Yuan, M.R., Liu, W.Q., Zhu, Y.F., and Xu, Y.J. (2014). *Russ. J. Electrochem.* 50: 1050.
28 Park, M.S., Lim, Y.G., Hwang, S.M. et al. (2014). *ChemSusChem* 7: 3138.
29 Ren, J.J., Su, L.W., Qin, X. et al. (2014). *J. Power Sources* 264: 108.
30 Park, C.M., Jo, Y.N., Park, J.W. et al. (2014). *Bull. Korean Chem. Soc.* 35: 2630.
31 Karthikeyan, K., Amaresh, S., Lee, S.N. et al. (2014). *ChemSusChem* 7: 2310.
32 Kaiyappan, K., Amaresh, S., and Lee, Y.S. (2014). *ACS Appl. Mater. Interfaces* 6: 11357.
33 Amatucci, G.G., Badway, F., Du Pasquier, A., and Zheng, T. (2001). *J. Electrochem. Soc.* 148: A930.
34 Kim, H., Park, K.Y., Cho, M.Y. et al. (2014). *ChemElectroChem* 1: 125.
35 Ren, J., Zhang, Y., Bai, W.Y. et al. (2014). *Angew. Chem. Int. Ed.* 53: 7864.
36 Kim, M., Xu, F., Lee, J.H. et al. (2014). *J. Mater. Chem. A* 2: 10029.
37 Barcellona, S., Ciccarelli, F., Iannuzzi, D., and Piegari, L. (2014). *IEEE Trans. Sustainable Energy* 5: 785.
38 Pan, S.W., Zhang, Z.T., Weng, W. et al. (2014). *Mater. Today* 17: 276.
39 Aravindan, V., Sundaramurthy, J., Jain, A. et al. (1858). *ChemSusChem* 2014: 7.
40 Lotfabad, E.M., Ding, J., Cui, K. et al. (2014). *ACS Nano* 8: 7115.
41 Zhu, J., Xu, Z., and Lu, B.N. (2014). *Nano Energy* 7: 114.
42 Tian, L.L., Wei, X.Y., Zhuang, Q.C. et al. (2014). *Nanoscale* 6: 6075.
43 Ahn, S.K., Yang, J.J., Kim, H.I. et al. (2014). *Chem. Lett.* 43: 898.
44 Yuan, M.R., Liu, W.Q., Zhu, Y.F., and Xu, Y.J. (2014). *Russ. J. Electrochem.* 50: 594.
45 Ohki, Y. (2014). *IEEE Electr. Insul. Mag.* 30: 54.
46 Xu, J., Mi, C.C., Cao, B.G. et al. (2014). *IEEE Trans. Veh. Technol.* 63: 1614.
47 Zhang, J., Shi, Z.Q., and Wang, C.Y. (2014). *Electrochim. Acta* 125: 22.
48 Naskar, P., Kundu, D., Maiti, A. et al. (2021). *ChemElectroChem* 8: 1393.
49 Tanaka, K., Ohzeki, K., Yamabe, T., and Yata, S. (1984). *Synth. Met.* 9: 41.
50 Yata, S., Hato, Y., Sakurai, K. et al. (1987). *Synth. Met.* 18: 645.
51 Li, G., Yang, Z., Yin, Z. et al. (2019). *J. Mater. Chem. A* 7: 15541.
52 Naoi, K., Ishimoto, S., Miyamoto, J.-i., and Naoi, W. (2012). *Energy Environ. Sci.* 5: 9363.
53 Pasquier, A.D., Plitz, I., Gural, J. et al. (2004). *J. Power Sources* 136: 160.
54 Hosaka, T., Kubota, K., Hameed, A.S., and Komaba, S. (2020). *Chem. Rev.* 120: 6358.
55 Peña, O. (2015). *Physica C* 514: 95–112.
56 Levi, E. and Aurbach, D. (2010). *Chem. Mater.* 22: 3678–3692.
57 Wan, L.F., Perdue, B.R., Apblett, C.A., and Prendergast, D. (2015). *Chem. Mater.* 27: 5932–5940.

58 Liang, Y., Feng, R., Yang, S. et al. (2011). *Adv. Mater.* 23: 640–643.
59 Liu, B., Luo, T., Mu, G. et al. (2013). *ACS Nano* 7: 8051–8058.
60 Kaewmaraya, T., Ramzan, M., Osorio-Guillén, J.M., and Ahuja, R. (2014). *Solid State Ionics* 261: 17–20.
61 Patridge, C.J., Wu, T.L., Jaye, C. et al. (2010). *Nano Lett.* 10: 2448–2453.
62 Ling, C., Zhang, R., Arthur, T.S., and Mizuno, F. (2015). *Chem. Mater.* 27: 5799–5807.
63 Spahr, M.E., Novak, P., Haas, O., and Nesper, R. (1995). *J. Power Sources* 54: 346–351.
64 Novak, P. and Desilvestro, J. (1993). *J. Electrochem. Soc.* 140: 140–144.
65 Tao, Z.L., Xu, L.N., Gou, X.L. et al. (2004). *Chem. Commun.* 2080–2081.
66 Su, S., Huang, Z., NuLi, Y. et al. (2015). *Chem. Commun.* 51: 2641–2644.
67 Kim, H.S., Arthur, T.S., Allred, G.D. et al. (2011). *Nat. Commun.* 2: 427.
68 Tian, H., Gao, T., Li, X. et al. (2017). *Nat. Commun.* 8: 14083.
69 NuLi, Y., Zheng, Y., Wang, F. et al. (2011). *Electrochem. Commun.* 13: 1143–1146.
70 Orikasa, Y., Masese, T., Koyama, Y. et al. (2014). *Sci. Rep.* 4: 5622.
71 Kuang, C., Zeng, W., and Li, Y. (2019). *J. Nanosci. Nanotechnol.* 19: 12–25.
72 Park, M.S., Kim, J.G., Kim, Y.J. et al. (2015). *Isr. J. Chem.* 55: 570–585.
73 Ling, C., Banerjee, D., and Matsui, M. (2012). *Electrochim. Acta* 76: 270–274.
74 Arthur, T.S., Singh, N., and Matsui, M. (2012). *Electrochem. Commun.* 16: 103–106.
75 Malyi, O.I., Tan, T.L., and Manzhos, S. (2013). *J. Power Sources* 233: 341–345.
76 Wang, Z., Su, Q., Shi, J. et al. (2014). *ACS Appl. Mater. Interfaces* 6: 6786–6789.
77 Er, D., Detsi, E., Kumar, H., and Shenoy, V.B. (2016). *ACS Energy Lett.* 1: 638–645.
78 Banerjee, S. and Pati, S.K. (2016). *Chem. Commun.* 52: 8381–8384.
79 Wu, N., Lyu, Y.C., Xiao, R.J. et al. (2014). *NPG Asia Mater.* 6: e120.
80 Aurbach, D., Lu, Z., Schechter, A. et al. (2000). *Nature* 407: 724–727.
81 Gregory, T.D., Hoffman, R.J., and Winterton, R.C. (1990). *J. Electrochem. Soc.* 137: 775–780.
82 Muldoon, J., Bucur, C.B., Oliver, A.G. et al. (2013). *Energy Environ. Sci.* 6: 482–487.
83 Zhang, H., Cao, D., and Bai, X. (2019). *J. Power Sources* 444: 227299.
84 Zhang, H., Ye, K., Zhu, K. et al. (2017). *Chem. Eur. J.* 23: 17118–17126.
85 Nam, K.W., Kim, S., Lee, S. et al. (2015). *Nano Lett.* 15: 4071–4079.
86 Mizuno, Y., Okubo, M., Hosono, E. et al. (2013). *J. Phys. Chem. C* 117: 10877–10882.
87 Yoo, H.D., Shterenberg, I., Gofer, Y. et al. (2014). *J. Electrochem. Soc.* 161: A410–A415.
88 Sun, Y., Chen, H., Xing, Y. et al. (2018). *Colloids Surf., A* 553: 539–545.
89 Zhang, H., Ye, K., Zhu, K. et al. (2017). *ACS Sustainable Chem. Eng.* 5: 6727–6735.
90 Cao, X., Wang, L., Chen, J., and Zheng, J. (2018). *ChemElectroChem* 5: 2789–2794.

91 Tian, Z., Tong, X., Sheng, G. et al. (2019). *Nat. Commun.* 10: 4913.
92 Juran, T.R. and Smeu, M. (2017). *Phys. Chem. Chem. Phys.* 19: 20684–20690.
93 Lipson, A.L., Pan, B., Lapidus, S.H. et al. (2015). *Chem. Mater.* 27: 8442–8447.
94 Ponrouch, A., Frontera, C., Bardé, F., and Palacín, M.R. (2016). *Nat. Mater.* 15: 169–172.
95 Ponrouch, A., Tchitchekova, D., Frontera, C. et al. (2016). *Electrochem. Commun.* 66: 75–78.
96 Aurbach, D., Skaletsky, R., and Gofer, Y. (1991). *J. Electrochem. Soc.* 138: 3536–3545.
97 Wang, D., Gao, X., Chen, Y. et al. (2018). *Nat. Mater.* 17: 16–20.
98 Shyamsunder, A., Blanc, L.E., Assoud, A., and Nazar, L.F. (2019). *ACS Energy Lett.* 4: 2271–2276.
99 Li, Z., Fuhr, O., Fichtner, M., and Zhao-Karger, Z. (2019). *Energy Environ. Sci.* 12: 3496–3501.
100 Ta, K., Zhang, R., Shin, M. et al. (2019). *ACS Appl. Mater. Interfaces* 11: 21536–21542.
101 Lee, C. and Jeong, S.K. (2018). *Electrochim. Acta* 265: 430–436.
102 Wu, N., Yao, W., Song, X. et al. (2019). *Adv. Energy Mater.* 9: 1803865.
103 Konarov, A., Voronina, N., Jo, J.H. et al. (2018). *ACS Energy Lett.* 3: 2620–2640.
104 Zhou, Z., Zhou, X., Zhang, M. et al. (2020). *Small* 16: 2003174.
105 Han, S.D., Kim, S., Li, D. et al. (2017). *Chem. Mater.* 29: 4874–4884.
106 Tian, Y., Amal, R., and Wang, D.W. (2016). *Front. Energy Res.* 4: 34.
107 Wang, H., Wang, M., and Tang, Y. (2018). *Energy Storage Mater.* 13: 1.
108 Wang, F., Borodin, O., Gao, T. et al. (2018). *Nat. Mater.* 17: 543.
109 Zhang, H., Liu, Q., Fang, Y. et al. (2019). *Adv. Mater.* 31: 1904948.
110 Chen, S., Ma, L., Zhang, K. et al. (2019). *J. Mater. Chem. A* 7: 7784.
111 Maughan, P.A., Tapia-Ruiz, N., and Bimbo, N. (2020). *Electrochim. Acta* 341: 136061.
112 Huang, Z., Chen, A., Mo, F. et al. (2020). *Adv. Energy Mater.* 10: 2001024.
113 Sun, G., Xiao, Y., Lu, B. et al. (2020). *ACS Appl. Mater. Interfaces* 12: 7239.
114 Yin, J., Zhang, W., Wang, W. et al. (2020). *Adv. Energy Mater.* 10: 2001705.
115 Li, J., Wang, N., Tian, J. et al. (2018). *Adv. Funct. Mater.* 28: 1806153.
116 Yin, J., Zhang, W., Alhebshi, N.A. et al. (2020). *Small Methods* 4: 1900853.
117 Holleck, G.L. (1972). *J. Electrochem. Soc.* 119: 1158–1161.
118 Karpinski, Z.J. and Osteryoung, R.A. (1984). *Inorg. Chem.* 23: 1491–1494.
119 Zhang, X. and Devine, T.M. (2006). *J. Electrochem. Soc.* 153: B375–B383.
120 Sun, H., Wang, W., Yu, Z. et al. (2015). *Chem. Commun.* 51: 11892–11895.
121 Lin, M.C., Gong, M., Lu, B. et al. (2015). *Nature* 520: 324–328.
122 Lei, H., Tu, J., Tian, D., and Jiao, S. (2018). *New J. Chem.* 42: 15684–15691.
123 Wang, F., Liu, Z., Wang, X. et al. (2016). *J. Mater. Chem. A* 4: 5115–5123.
124 Li, K., Shao, Y., Liu, S. et al. (2017). *Small* 13: 1700380.
125 Li, H.S., Zhang, X., Zhao, Z.C. et al. (2020). *Energy Storage Mater.* 26: 83.
126 Zhu, J.H., Roscow, J., Chandrasekaran, S. et al. (2020). *ChemSusChem* 13: 1275.
127 Wang, L., Yang, G.R., Peng, S.J. et al. (2020). *Energy Storage Mater.* 25: 443.
128 Meng, F., Long, T., Xu, B. et al. (2020). *Front. Chem.* 8: 652.

129 Chen, J.T., Yang, B.J., Liu, B. et al. (2019). *Curr. Opin. Electrochem.* 18: 1.
130 Jia, R., Shen, G.Z., and Chen, D. (2020). *Sci. China Mater.* 63: 185.
131 Zhai, H.F., Xia, B.Y., and Park, H.S. (2019). *J. Mater. Chem. A* 7: 22163.
132 Zhao, X.Y., Zhang, Y.B., Wang, Y.F., and Wei, H.G. (2019). *Batteries Supercaps* 2: 899.
133 Han, D.L., Zhang, J., Weng, Z. et al. (2019). *Mater. Today Energy* 11: 30.
134 Kim, J., Choi, M.S., Shin, K.H. et al. (2019). *Adv. Mater.* 31: 20.
135 Zhang, T.Y., Yang, L., Yan, X.B., and Ding, X. (2018). *Small* 14: 20.
136 Glushenkov, A.M. and Ellis, A.V. (2018). *Adv. Sustainable Syst.* 2: 25.
137 Ding, J., Hu, W.B., Paek, E., and Mitlin, D. (2018). *Chem. Rev.* 118: 6457.
138 Li, F. and Zhou, Z. (2018). *Small* 14: 25.
139 He, Y.Z., Han, X.J., Du, Y.C. et al. (2018). *Nano Res.* 11: 2573.
140 Ding, J., Wang, H.L., Li, Z. et al. (2015). *Energy Environ. Sci.* 8: 941.
141 Ruan, J.F., Yuan, T., Pang, Y.P. et al. (2018). *Carbon* 126: 9.
142 Qie, L., Chen, W.M., Xiong, X.Q. et al. (2015). *Adv. Sci.* 2: 6.
143 Wang, X.L., Li, G., Hassan, F.M. et al. (2015). *Nano Energy* 15: 746.
144 Li, D.D., Zhang, L., Chen, H.B. et al. (2016). *J. Mater. Chem. A* 4: 8630.
145 Lu, M.J., Yu, W.H., Shi, J. et al. (2017). *Electrochim. Acta* 251: 396.
146 Zou, L., Lai, Y.Q., Hu, H.X. et al. (2017). *Chem. Eur. J.* 23: 14261.
147 Simon, P., Gogotsi, Y., and Dunn, B. (2014). *Science* 343: 1210.
148 Nishihara, H. and Kyotani, T. (2012). *Adv. Mater.* 24: 4473.
149 Zhao, L.P., Qi, L., and Wang, H.Y. (2013). *J. Power Sources* 242: 597.
150 Gonzalez-Gil, A., Palacin, R., and Batty, P. (2013). *Energy Convers. Manage.* 75: 374.
151 Ding, J., Li, Z., Cui, K. et al. (2016). *Nano Energy* 23: 129.
152 Xu, J.T., Wang, M., Wickramaratne, N.P. et al. (2015). *Adv. Mater.* 27: 2042.
153 Seh, Z.W., Li, W.Y., Cha, J.J. et al. (2013). *Nat. Commun.* 4: 6.
154 Wang, Y.P., Zhao, K.J., Wang, K. et al. (2020). *J. Alloys Compd.* 844: 8.
155 Han, M., Srivastava, S.B., Yildiz, E. et al. (2020). *ACS Appl. Mater. Interfaces* 12: 42997.
156 Yan, H.X., Yang, M., Liu, L. et al. (2020). *J. Alloys Compd.* 843: 9.
157 Li, Y.Z., Wang, H.W., Wang, L.B. et al. (2019). *Small* 15: 13.
158 Dong, S.Y., Shen, L.F., Li, H.S. et al. (2016). *Adv. Funct. Mater.* 26: 3703.
159 Que, L.F., Yu, F.D., He, K.W. et al. (2017). *Chem. Mater.* 29: 9133.
160 Xu, D.M., Chao, D.L., Wang, H.W. et al. (2018). *Adv. Energy Mater.* 8: 11.
161 Li, H., Peng, L., Zhu, Y. et al. (2016). *Nano Lett.* 16: 5938.
162 Moeez, I., Jung, H.G., Lim, H.D., and Chung, K.Y. (2019). *ACS Appl. Mater. Interfaces* 11: 41394.
163 Zou, K.Y., Cai, P., Liu, C. et al. (2019). *J. Mater. Chem. A* 7: 13540.
164 Zou, K.Y., Cai, P., Tian, Y. et al. (2020). *Small Methods* 4: 8.